

Research Paper

Gold Nanoparticles' Morphology Affects Blood Flow near a Wavy Biological Tissue Wall: An Application for Cancer Therapy

Ji-Huan He¹, Nasser S. Elgazery², Nader Y. Abd Elazem³

¹ National Engineering Laboratory for Modern Silk, College of Textile and Clothing Engineering, Soochow University, Suzhou, China, Email: hejihuan@suda.edu.cn

² Department of Mathematics, Faculty of Education, Ain Shams University, El Makrizy St, Roxy, Heliopolis:11566, Cairo, Egypt, Email: nasersaleh@edu.asu.edu.eg

³ Department of Basic Science, Cairo Higher Institute for Engineering, Computer Science and Management, New Cairo, Cairo, Egypt, Email: nader.yabdelazem@chi.edu.eg

Received September 03 2023; Revised November 18 2023; Accepted for publication December 23 2023.

Corresponding author: N.Y. Abd Elazem (nader.yabdelazem@chi.edu.eg; naderelnafrawy@yahoo.com; nader_47@hotmail.com)

© 2023 Published by Shahid Chamran University of Ahvaz

Abstract. The purpose of this study is to look at how gold nanoparticles affect the circulation near wavy biological cell walls. Non-linear thermal radiation was found to enhance the heat transfer rates of nanofluid flow by numerical calculations. The mathematical model was a temporally magnetized non-Newtonian Casson micropolar nanofluid flow through a heated vertical wavy surface. The importance of predicting heat and mass transfer for irregular surfaces cannot be overstated, as irregular surfaces are common in many applications, including refrigerator condensers and flat-plate solar collectors. For this reason, it is imperative to study heat and mass transfer in complex geometries. Furthermore, the fluid temperature factors like nanofluid viscosity and microrotation viscosity were taken into account. A graph comparing the published data and the present numerical computation revealed an exact match. A physical interpretation of images was provided to describe the phenomenon of blood flow by heat transfer according to various circumstances. In medical treatment, especially cancer therapy, these results are crucial. Gold nanoparticles are among the best particles because they are stable metallic nanoparticles with excellent catalytic, magnetic, and optical properties. The investigation's findings showed that as time-steps grow, each profile's effectiveness tends to decrease, moving the unstable condition closer to the steady state. Whereas, the sphere-shaped nanoparticles have a significant effect on temperature profile change, column-shaped nanoparticles have less effect. Local skin friction rises and the local Nusselt number falls when the values of the two surface amplitude parameters rise.

Keywords: Non-linear thermal radiation; blood-intervened gold nanoparticles; heated wavy surface; variable nanofluid and micro rotation viscosities; Implicit Chebyshev pseudo spectral (ICPS) method.

1. Introduction

The creation of a model of non-Newtonian fluids that can be used to study the behavior of different fluids, particularly blood, is most suitable for the research of thermo-micropolar and micropolar fluids [1-3]. According to Elgazery [4], the permeability of porous membranes increases the spreading of fluids.

Many studies have been conducted with blood, described as a non-Newtonian micropolar fluid. Chaturani and Upadhyaya [5] used the micropolar fluid model to conduct a theoretical study of blood flow inside a very narrow tube. Mekheimer and El Kot [6], Abdullah and Amin [7], and Ellahi et al. [8] used micropolar fluid in the presence of stenosis to investigate blood flow in a tapered artery. Ellahi et al. [9] investigated the effect of mass and heat transfer on blood flow via micropolar fluid in the presence of permeable walls and a tapered stenosed artery. Blood flow was investigated by Mekheimer et al. [10] for the simultaneous effects of metallic nanoparticles and the magnetic field in a stenotic artery using the micropolar fluid model as blood flow. Muthu et al. [11] also investigated the oscillatory blood flow through an annular tube using a micropolar fluid model. Misra et al. [12] examined an oscillatory electro-osmotic for blood flow through a microchannel using the micropolar fluid model. Asha and Deepa [13] studied how thermal radiation and entropy generation affect the peristaltic motion of blood flow in a tapered channel as a micropolar fluid. The majority of physiological fluids in the human body exhibit non-Newtonian behavior. Blood is a complex mixture (plasma) of gases, salts, proteins, carbohydrates, and lipids that contains suspended red blood cells (erythrocytes), white blood cells (leukocytes), and platelets. Ninety percent of plasma is water, making it a Newtonian fluid. However, blood is widely believed to be a non-Newtonian fluid made up of blood plasma and blood cells. Many mathematical models have been established in numerous investigations to describe the rheological behavior of blood. Karvelas et al. [14] explored the effect of micropolar fluid properties on blood flow in a human carotid model. However, numerous other studies rely on describing blood as a non-Newtonian Casson fluid, such as [15-21].

Many recent studies have combined the micropolar fluid and Casson models to produce more accurate and realistic results. Using the Keller box numerical approach, Iqbal et al. [22] examined blood flow (micropolar Casson fluid model) along a stretching



plate in response to the action of a magnetic field with a slope. In the presence of internal heating, Mehmood et al. [23] used the Runge Kutta Fehlberg numerical technique with a shooting algorithm to study blood flow as a micropolar Casson model near a stretching sheet. Ali et al. [24] conducted a numerical study of magneto-pulsating blood flow (micropolar Casson fluid) in a constricted channel through a Darcian porous medium. Blood flow was also described by Elelmy et al. [25] using the Casson-micropolar nanofluid model. Moreover, Amjad et al. [26] studied blood flow as a Casson-micropolar nanofluid close to a curved permeable stretching sheet under an induced magnetic field and Lorentz force. One of the most severe and deadly illnesses that can affect a person is cancer. Over the past few decades, there have been many attempts to combat cancer, and our understanding of the disease has gradually increased. The only available cancer treatments at the moment are radiation, chemotherapy, and surgery, despite our best efforts. Using nanotechnology to administer a variety of pharmaceuticals is one possible answer within the context of these major efforts in this field. The goal of these initiatives is to use gold nanoparticles for cancer treatments and as diagnostic instruments [27].

In recent times, gold nanoparticles have been extensively employed across multiple domains, especially in the highest degree of illness therapy [28]. The study conducted by Mekheimer et al. [29] examined the effects of gold nanoparticles on peristaltic blood flow via a catheter. Gold nanoparticles injected into blood flow inside a porous medium were studied by Eldabe et al. [30]. Additionally, blood flow with gold nanoparticles inside a stenosed vessel under a variable nanofluid viscosity effect was covered by Elnaqeeb et al. [31]. Using blood-intervened gold nanoparticles, Mekheimer et al. [32] clarified the antibacterial effects of electrothermal transport in an osmosis-electro artery with overlapping stenosis. Recent research has examined the impact of wall characteristics on the results of magneto-blood-intervened gold nanoparticles passing through a wavy tube [33].

According to He and Abd Elazem's findings [34], for the stretched sheet, the thickness of the thermal barrier layer grows as the radiation parameter increases, which lowers the heat transfer rate. The results have applications in many domains, such as biomedical, thermo-mechanical processes, and the best heat transfer structure for a renewable energy collecting system. The results in Ref. [35] show that only when the slender needle moves against the direction of the free stream are the dual similarity solutions produced. Furthermore, the range of the velocity ratio parameter for which the solution exists is decreased by the mass of the second nanoparticle as well as the magnetic parameter. The findings in Ref. [36] show that while the temperature increases when the Joule heating increases with constant values of the electro-osmotic parameter and Helmholtz Smoluchowski velocity, the velocity increases as these parameters increase. Additionally, as the magnetic field is strengthened and the altitude of stenosis takes on bigger values, there is a difference in the profile of velocity to the blood flow. The findings in Ref. [37] demonstrate that the hyperbolicity of the model produces temperatures greater than those attained with a parabolic model because of laser-induced heat.

Furthermore, the significance of non-linear thermal radiation is beneficial for blood flow control during thermal surgery or therapy. As a result, taking into account blood flow containing gold nanoparticles with heat transfer in the presence of a magnetic field and non-linear thermal radiation becomes critical in biological and industrial processes, such as biomedical fluids, cancer therapy, cancer tumor treatment, biofluids in biological tissue, drug transportation, emulsions, lubricants, and nuclear fuel slurries [28].

One of the most significant non-Newtonian models that explains this behavior and exhibits the shear thinning property is the Casson fluid. The Casson fluid exhibits Newtonian behavior when the shear stress rises to a level significantly higher than the yield stress. Therefore, it is calculated that the Casson fluid fits the rheological data better than conventional models for viscoelastic fluids. On the other hand, ferrofluids, blood flows, bubbly liquids, liquid crystals, and so forth are examples of physical micropolar fluids. In recent times, numerous studies have integrated multiple models to depict non-Newtonian fluids, such as the Casson-Carreau, micropolar-Carreau, and micropolar-Maxwell models [25, 38–40]. Therefore, the purpose of this article study is to examine how the morphology of gold nanoparticles influences blood flow (blood with suspended gold (Au) nanoparticles) near a vertically heated wavy wall in the presence of non-linear thermal radiation and variable microrotation viscosity in the vicinity of a wavy biological tissue wall in the context of cancer therapy (esophageal cancer).

The majority of mathematical research on biological systems made the assumption that the wall was wavy, flat, cylinder-shaped, curved, or peristaltic [25, 41–48]. Consequently, we used the same methodology and took the wavy wall's shape into account in this investigation. The study's findings showed that as time steps increase, the efficacy of each profile tends to decrease, and the unstable state approaches the steady state. Furthermore, compared to earlier research, the steady state can be reached faster with the current numerical approach. The rate of heat transfer is controlled by columnar-shaped nanoparticles, while spherically-shaped nanoparticles have a lesser function.

2. Mathematical Formulations

This study attempts to investigate how gold nanoparticles' morphology affects blood flow near a wavy biological tissue wall, taking into account the following hypotheses:

- A temporal 2D magneto-non-Newtonian Casson-micropolar nanofluid (blood with suspended gold nanoparticles) flow close to a vertically heated wavy wall is assumed.
- In the present physical model, it is given that the wavy wall $\hat{\sigma}(\hat{x})$ is kept at a uniform temperature T_w greater than its corresponding values of ambient temperature T_∞ .
- It is also assumed that the viscosity and rotational viscosity of blood should be taken as functions of temperature, as shown in equations (12) and (13).
- It is also assumed that a uniform vertical magnetic field B_0^2 is utilized for the flow.
- It is also assumed that the term $\partial q_r / \partial \hat{y}$ represents the nonlinear thermal radiation that can be formed as equation (8).

As shown in Fig. 1, the heated wavy surface with a sinusoidal deviation is taken as [51, 52]:

$$\hat{y} = \hat{\sigma}(\hat{x}) = \hat{a}_1 \sin(2\pi\hat{x} / l) + \hat{a}_2 \sin(4\pi\hat{x} / l) \quad (1)$$

where l denotes the characteristic length. The distinct amplitudes of the wavy wall are \hat{a}_1 and \hat{a}_2 . The governing equations are listed below [53–56]:

$$\frac{\partial \hat{u}}{\partial \hat{x}} + \frac{\partial \hat{v}}{\partial \hat{y}} = 0, \quad (2)$$



$$\rho_{nf} \left(\frac{\partial \hat{u}}{\partial \hat{t}} + \hat{u} \frac{\partial \hat{u}}{\partial \hat{x}} + \hat{v} \frac{\partial \hat{u}}{\partial \hat{y}} \right) = -\frac{\partial \hat{P}}{\partial \hat{x}} + \frac{\partial}{\partial \hat{x}} \left[\mu_{nf}(T) + \frac{p_y}{\sqrt{2\pi_c}} + \kappa(T) \right] \frac{\partial \hat{u}}{\partial \hat{x}} + \frac{\partial}{\partial \hat{y}} \left[\mu_{nf}(T) + \frac{p_y}{\sqrt{2\pi_c}} + \kappa(T) \right] \frac{\partial \hat{u}}{\partial \hat{y}} + \kappa(T) \frac{\partial \hat{N}}{\partial \hat{y}} - \sigma_{nf} B_0^2 \hat{u} + \rho_{nf} g \beta_T (T - T_\infty), \quad (3)$$

$$\rho_{nf} \left(\frac{\partial \hat{v}}{\partial \hat{t}} + \hat{u} \frac{\partial \hat{v}}{\partial \hat{x}} + \hat{v} \frac{\partial \hat{v}}{\partial \hat{y}} \right) = -\frac{\partial \hat{P}}{\partial \hat{y}} + \frac{\partial}{\partial \hat{x}} \left[\mu_{nf}(T) + \frac{p_y}{\sqrt{2\pi_c}} + \kappa(T) \right] \frac{\partial \hat{v}}{\partial \hat{x}} + \frac{\partial}{\partial \hat{y}} \left[\mu_{nf}(T) + \frac{p_y}{\sqrt{2\pi_c}} + \kappa(T) \right] \frac{\partial \hat{v}}{\partial \hat{y}} - \kappa(T) \frac{\partial \hat{N}}{\partial \hat{x}}, \quad (4)$$

$$\rho_{nf} \left(\frac{\partial \hat{N}}{\partial \hat{t}} + \hat{u} \frac{\partial \hat{N}}{\partial \hat{x}} + \hat{v} \frac{\partial \hat{N}}{\partial \hat{y}} \right) = \kappa(T) \left(\frac{\partial \hat{v}}{\partial \hat{x}} - \frac{\partial \hat{u}}{\partial \hat{y}} - 2\hat{N} \right) + \frac{\partial}{\partial \hat{x}} \left(\Omega(T) \frac{\partial \hat{N}}{\partial \hat{x}} \right) + \frac{\partial}{\partial \hat{y}} \left(\Omega(T) \frac{\partial \hat{N}}{\partial \hat{y}} \right), \quad (5)$$

$$(\rho C_p)_{nf} \left(\frac{\partial T}{\partial \hat{t}} + \hat{u} \frac{\partial T}{\partial \hat{x}} + \hat{v} \frac{\partial T}{\partial \hat{y}} \right) = k_{nf} \left(\frac{\partial^2 T}{\partial \hat{x}^2} + \frac{\partial^2 T}{\partial \hat{y}^2} \right) - \frac{\partial q_r}{\partial \hat{y}}. \quad (6)$$

The boundary conditions are given by:

$$\begin{aligned} \hat{t} \leq 0: & \hat{u}(\hat{x}, \hat{y}, \hat{t} \leq 0) = \hat{v}(\hat{x}, \hat{y}, \hat{t} \leq 0) = \hat{N}(\hat{x}, \hat{y}, \hat{t} \leq 0) = 0, T(\hat{x}, \hat{y}, \hat{t} \leq 0) = T_\infty, \\ \hat{t} > 0: & \begin{cases} \hat{u}(\hat{x}, 0, \hat{t}) = \hat{v}(\hat{x}, 0, \hat{t}) = 0, T(\hat{x}, 0, \hat{t}) = T_w, \hat{N}(\hat{x}, 0, \hat{t}) = \frac{1}{2} \left(\frac{\partial \hat{v}}{\partial \hat{x}} - \frac{\partial \hat{u}}{\partial \hat{y}} \right)_{\hat{y}=0}, \\ \hat{u}(\hat{x}, \infty, \hat{t}) \rightarrow 0, T(\hat{x}, \infty, \hat{t}) \rightarrow T_\infty, \hat{N}(\hat{x}, \infty, \hat{t}) \rightarrow 0, \hat{P}(\hat{x}, \infty, \hat{t}) \rightarrow \hat{P}_\infty \text{ as } \hat{y} \rightarrow \infty. \end{cases} \end{aligned} \quad (7)$$

Here, \hat{P} and \hat{t} are the pressure and time. (\hat{u}, \hat{v}) , T , and \hat{N} are (\hat{x}, \hat{y}) -component velocities, temperature, and microrotation velocities, respectively. g and β_T are the acceleration due to gravity vector and thermal expansion coefficient. $\rho_{nf}, \sigma_{nf}, C_p$, and k_{nf} are the density, electrical conductivity, specific heat at constant pressure, and thermal conductivity of the nanofluid. π_c is the critical value of the product $e_{ij} e_{ij}$ and $e_{ij} = [\partial \hat{v}_i / \partial \hat{x}_j + \partial \hat{v}_j / \partial \hat{x}_i] / 2$ is the deformation rate. p_y is the yield stress of the nanofluid. T_∞ and T_w are also the blood temperatures far away from and near the wavy wall, respectively. $\kappa(T)$ and $\Omega(T)$ are the variable microrotation and spin gradient viscosities, respectively. j is the constant microinertia density (the microinertia, or unit mass). In equation (6), the term $\partial q_r / \partial \hat{y}$ represents the nonlinear thermal radiation that can be formed as [50, 56, 57]:

$$\frac{\partial q_r}{\partial \hat{y}} = -\frac{16\delta}{3\Delta} \left(T^3 \frac{\partial^2 T}{\partial \hat{y}^2} + 3T^2 \frac{\partial T}{\partial \hat{y}} \right) \quad (8)$$

where δ and Δ are the Stefan-Boltzmann constant and mean absorption coefficient. Furthermore, the thermophysical properties of the nanofluid can be expressed as [28, 54, 58, 59]:

$$\rho_{nf} = D_1 \rho_f, (\rho C_p)_{nf} = D_2 (\rho C_p)_f, \sigma_{nf} = D_3 \sigma_f, k_{nf} = D_4 k_f. \quad (9)$$

where,

$$\left. \begin{aligned} D_1 &= (1 - \varphi) + \frac{\rho_s}{\rho_f} \varphi, D_2 = (1 - \varphi) + \varphi \frac{(\rho C_p)_s}{(\rho C_p)_f}, \\ D_3 &= \frac{(\sigma_s + 2\sigma_f + 2\varphi(\sigma_s - \sigma_f))}{(\sigma_s + 2\sigma_f - \varphi(\sigma_s - \sigma_f))}, \\ D_4 &= \frac{[k_s + (m - 1)k_f] - (m - 1)(k_f - k_s)\varphi}{[k_s + (m - 1)k_f] + (k_f - k_s)\varphi}. \end{aligned} \right\} \quad (10)$$

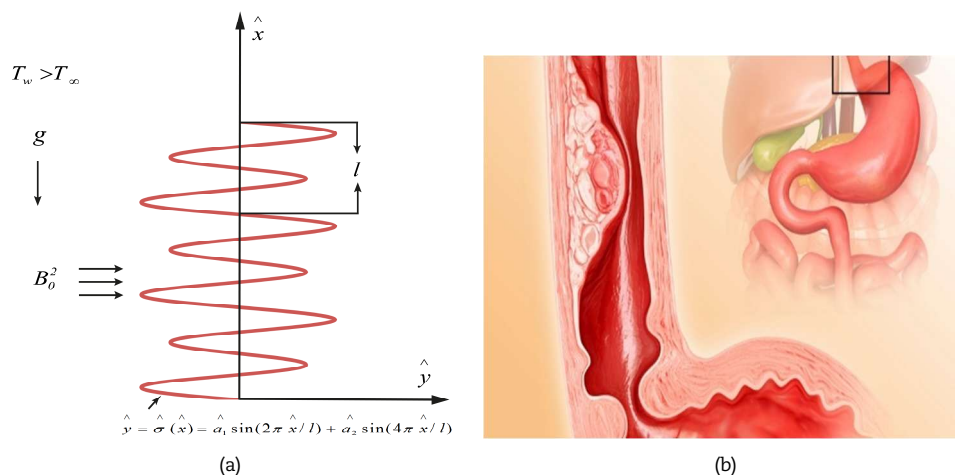


Fig. 1. (a) Geometry of flow along a wavy biological tissue wall; (b) Esophageal cancer [55].



Table 1. The shape-related parameter values of gold nanoparticles [28].

Shapes	Sphere	Tetrahedron	Hexahedron	Lamina	Column
φ	1	0.7387	0.8060	0.1857	0.4710
m	3	4.0613	3.7221	16.1576	6.3698

Table 2. The thermophysical properties of the blood and gold nanoparticles (Au) [27, 56].

	σ (s / m)	C_p (J / kg K)	ρ (kg / m ³)	k (W / m K)
Gold (Au)	4.1×10^6	129	19300	318
Blood	1090	3617	1050	0.52

Here, φ and m are the volume fraction and shape factor of the gold nanoparticle as presented in Table 1. The two indices f and s also refer to blood as a base fluid and gold nanoparticles (Au) (see Table 2 for the thermophysical properties of the blood and gold nanoparticles [27, 56]).

Utilizing the dimensionless variables [50, 52]:

$$\left. \begin{aligned} x &= \frac{\hat{x}}{l}, y = \frac{\hat{y} - \hat{\sigma}}{l} Gr^{1/4}, t = \frac{\mu_0 \hat{t}}{\rho_f l^2} Gr^{1/2}, u = \frac{l \hat{u} \rho_f}{\mu_0} Gr^{-1/2}, v = \frac{l(\hat{v} - \hat{\sigma}_x \hat{u}) \rho_f}{\mu_0} Gr^{-1/4}, \\ N &= \frac{l^2 \hat{N} \rho_f}{\mu_0} Gr^{-3/4}, \theta = \frac{T - T_\infty}{T_w - T_\infty}, P = \frac{l^2 (\hat{P} - \hat{P}_\infty)}{\rho_f \nu_0^2} Gr^{-1}, \\ \alpha_1 &= \frac{\hat{\alpha}_1}{l}, \alpha_2 = \frac{\hat{\alpha}_2}{l}, \sigma = \frac{\hat{\sigma}}{l}, \hat{\sigma}_x = \frac{d\hat{\sigma}}{d\hat{x}}, \frac{d\sigma}{dx}, \hat{\sigma}_{xx} = \frac{d\hat{\sigma}_x}{d\hat{x}}. \end{aligned} \right\} \quad (11)$$

Furthermore, for more accuracy, the viscosity and rotational viscosity of blood should be taken as functions of temperature in the following forms: [27, 54]:

$$\mu_{nf}(T) = D_5 \mu_0 e^{-\beta_1 \theta}, \quad (12)$$

$$\kappa(T) = \kappa_0 e^{-\beta_2 \theta}, \quad (13)$$

where,

$$D_5 = (123\varphi^2 + 7.3\varphi + 1), \varphi > 0.02. \quad (14)$$

Here, μ_0 and κ_0 are the constant viscosity and constant microrotation viscosity. β_1 and β_2 also the variable blood viscosity and variable microrotation viscosity parameters. Consequently, the variable spin gradient viscosity will be rewritten as: $\Omega(T) = (\mu_{nf}(T) + \kappa(T) / 2)j$. The undulating surface can be made flat by using the straightforward coordinate transformation mentioned above. After that, the dimensionless governing system can be produced as follows by taking, $\partial P / \partial x = 0$, eliminating, $\partial P / \partial y$, and disregarding the small-order terms in the Grashof number Gr (see [51, 60]).

Subsequently, the governing system (2)-(7) with the help of Eqs. (12)-(14), can be written in the following dimensionless system:

$$\frac{\partial u}{\partial x} + \frac{\partial v}{\partial y} = 0 \quad (15)$$

$$\begin{aligned} \frac{\partial u}{\partial t} + u \frac{\partial u}{\partial x} + v \frac{\partial u}{\partial y} &= -\frac{1}{D_1} \frac{\partial P}{\partial x} + \frac{\sigma_x}{D_1} \frac{\partial P}{\partial y} Gr^{1/4} + \frac{\bar{R}}{D_1} e^{-\beta_2 \theta} \frac{\partial N}{\partial y} - \frac{D_3}{D_1} M u + \theta \\ &+ (1 + \sigma_x^2) \left[\left(\frac{D_5}{D_1} e^{-\beta_1 \theta} + \frac{1}{D_1} \cdot \frac{1}{\beta} + \frac{\bar{R}}{D_1} e^{-\beta_2 \theta} \right) \frac{\partial^2 u}{\partial y^2} - \left(\frac{D_5}{D_1} \beta_1 e^{-\beta_1 \theta} + \frac{\bar{R}}{D_1} \beta_2 e^{-\beta_2 \theta} \right) \frac{\partial u}{\partial y} \cdot \frac{\partial \theta}{\partial y} \right], \end{aligned} \quad (16)$$

$$\begin{aligned} \frac{\sigma_x}{D_1} \frac{\partial P}{\partial y} Gr^{1/4} + \sigma_x^2 \left(\frac{\partial u}{\partial t} + u \frac{\partial u}{\partial x} + v \frac{\partial u}{\partial y} \right) + \sigma_x \sigma_{xx} u^2 &= \frac{\bar{R}}{D_1} \sigma_x^2 \frac{\partial N}{\partial y} \\ &+ \sigma_x^2 (1 + \sigma_x^2) \left[\left(\frac{D_5}{D_1} e^{-\beta_1 \theta} + \frac{1}{D_1} \cdot \frac{1}{\beta} + \frac{\bar{R}}{D_1} e^{-\beta_2 \theta} \right) \frac{\partial^2 u}{\partial y^2} - \left(\frac{D_5}{D_1} \beta_1 e^{-\beta_1 \theta} + \frac{\bar{R}}{D_1} \beta_2 e^{-\beta_2 \theta} \right) \frac{\partial u}{\partial y} \cdot \frac{\partial \theta}{\partial y} \right], \end{aligned} \quad (17)$$

$$D_1 \left[\frac{\partial N}{\partial t} + u \frac{\partial N}{\partial x} + v \frac{\partial N}{\partial y} \right] = (1 + \sigma_x^2) \left[\left(\frac{D_5}{D_1} e^{-\beta_1 \theta} + \frac{\bar{R}}{2} e^{-\beta_2 \theta} \right) \frac{\partial^2 N}{\partial y^2} - \left(\frac{D_5}{D_1} \beta_1 e^{-\beta_1 \theta} + \frac{\bar{R}}{2} \beta_2 e^{-\beta_2 \theta} \right) \frac{\partial N}{\partial y} \cdot \frac{\partial \theta}{\partial y} \right] - \bar{R} B e^{-\beta_2 \theta} \left((1 + \sigma_x^2) \frac{\partial u}{\partial y} + 2N \right), \quad (18)$$

$$D_2 Pr \left[\frac{\partial \theta}{\partial t} + u \frac{\partial \theta}{\partial x} + v \frac{\partial \theta}{\partial y} \right] = D_4 (1 + \sigma_x^2) \frac{\partial^2 \theta}{\partial y^2} + \frac{4}{3} Ra \left[3r(1 + r\theta)^2 \left(\frac{\partial \theta}{\partial y} \right)^2 + (1 + r\theta)^3 \frac{\partial^2 \theta}{\partial y^2} \right]. \quad (19)$$

Subject to the following boundary conditions:



$$\begin{aligned}
 t \leq 0: & \quad u(x, y, t \leq 0) = v(x, y, t \leq 0) = N(x, y, t \leq 0) = \theta(x, y, t \leq 0) = 0, \\
 t > 0: & \quad \begin{cases} u(x, 0, t) = v(x, 0, t) = 0, \theta(x, 0, t) = 1, N(x, 0, t) = -\frac{1}{2}(1 + \sigma_x^2) \left(\frac{\partial u}{\partial y} \right)_{y=0} \\ u(x, \infty, t) \rightarrow 0, \theta(x, \infty, t) \rightarrow 0, N(x, \infty, t) \rightarrow 0, P(x, \infty, t) \rightarrow 0. \end{cases} \quad (20)
 \end{aligned}$$

As well as in Eqs. (16) and (17), ignore the small-order terms in, Gr , eliminate $(Gr^{1/4} \sigma_x / D_1)(\partial P / \partial y)$, and take $\partial P / \partial x = 0$ [52, 61], then the momentum equation can be rewritten in the following dimensionless form:

$$\begin{aligned}
 D_1 \left[\frac{\partial u}{\partial t} + \frac{\sigma_x \sigma_{xx}}{1 + \sigma_x^2} u^2 + u \frac{\partial u}{\partial x} + v \frac{\partial u}{\partial y} \right] &= \bar{R} \frac{\partial N}{\partial y} + \frac{1}{(1 + \sigma_x^2)} (D_1 \theta - D_3 M u) \\
 &+ (1 + \sigma_x^2) \left\{ \left[D_5 e^{-\beta_1 \theta} + \frac{1}{\beta} + \bar{R} e^{-\beta_2 \theta} \right] \frac{\partial^2 u}{\partial y^2} - (D_5 \beta_1 e^{-\beta_1 \theta} + \bar{R} \beta_2 e^{-\beta_2 \theta}) \frac{\partial u}{\partial y} \cdot \frac{\partial \theta}{\partial y} \right\}. \quad (21)
 \end{aligned}$$

where $\beta = \mu_0 \sqrt{2\pi_c} / p_y$ and $\bar{R} = \kappa_0 / \mu_0$ are the upper limit apparent nanofluid viscosity coefficient and dimensionless microrotation parameters, respectively. It is noticeable that, for $\bar{R} \rightarrow 0$ and $\beta \rightarrow \infty$, the blood model tends to a Newtonian one. $M = (\sigma_f B_0^2 l^2 / \mu_0) Gr^{-1/2}$ is the dimensionless magnetic field parameter, and $Gr = [l^2 g \beta_r (\hat{P} - \hat{P}_\infty)] / \nu_0^2$ is the Grashof number. $B = (l^2 / j) Gr^{-1/2}$ is a dimensionless parameter, and $\nu_0 = \mu_0 / \rho_f$ is the blood kinematic viscosity. $Ra = (4\delta T_\infty^3) / (3\Delta k_f)$ and $r = [T_w / T_\infty] - 1$ are the non-linear thermal radiation and relative temperature difference within blood flow parameters, respectively. Here, when the blood temperature take 310 Kelvin, $k_0 = 2.2 \times 10^3 J / ms$ Kelvin, $C_p = 14.65 J / kg$ Kelvin, and $\mu_0 = 3.2 \times 10^3 kg / ms$, then the blood Prandtl number $Pr = [\mu_0 (C_p)_f] / k_0$ can equal approximately 21 [25].

The following transformation should be used to convert the current complex wavy wall to another flat plate and remove the singularity at the leading edge [49, 51, 53, 62, 63]:

$$\tau = t(4x)^{-1/2}, X = x, Y = y(4x)^{-1/4}, U = u(4x)^{-1/2}, V = v(4x)^{1/4}, \bar{N} = N(4x)^{-1/4}. \quad (22)$$

Therefore, in view of transformation (22), Eqs. (15), (18), (19), and (21) will reduce to the following convenient form:

$$2U + 4X \frac{\partial U}{\partial X} - Y \frac{\partial U}{\partial Y} + \frac{\partial V}{\partial Y} = 0, \quad (23)$$

$$\begin{aligned}
 D_1 \left[\frac{\partial U}{\partial \tau} + 4XU \frac{\partial U}{\partial X} + (V - YU) \frac{\partial U}{\partial Y} + \left(2 + \frac{4X\sigma_x \sigma_{xx}}{1 + \sigma_x^2} \right) U^2 \right] &= \bar{R} \frac{\partial \bar{N}}{\partial Y} + \frac{1}{(1 + \sigma_x^2)} (D_1 \theta - D_3 (4X)^{1/2} M U) \\
 &+ (1 + \sigma_x^2) \left\{ \left[D_5 e^{-\beta_1 \theta} + \frac{1}{\beta} + \bar{R} e^{-\beta_2 \theta} \right] \frac{\partial^2 U}{\partial Y^2} - (D_5 \beta_1 e^{-\beta_1 \theta} + \bar{R} \beta_2 e^{-\beta_2 \theta}) \frac{\partial U}{\partial Y} \cdot \frac{\partial \theta}{\partial Y} \right\}, \quad (24)
 \end{aligned}$$

$$\begin{aligned}
 D_1 \left[\frac{\partial \bar{N}}{\partial \tau} + 4XU \frac{\partial \bar{N}}{\partial X} + (V - YU) \frac{\partial \bar{N}}{\partial Y} + U \bar{N} \right] &= -\bar{R} B e^{-\beta_2 \theta} (4X)^{1/2} \left((1 + \sigma_x^2) \frac{\partial U}{\partial Y} + 2 \bar{N} \right) \\
 &+ (1 + \sigma_x^2) \left\{ \left[D_5 e^{-\beta_1 \theta} + \frac{\bar{R}}{2} e^{-\beta_2 \theta} \right] \frac{\partial^2 \bar{N}}{\partial Y^2} - \left(D_5 \beta_1 e^{-\beta_1 \theta} + \frac{\bar{R}}{2} \beta_2 e^{-\beta_2 \theta} \right) \frac{\partial \bar{N}}{\partial Y} \cdot \frac{\partial \theta}{\partial Y} \right\}, \quad (25)
 \end{aligned}$$

$$D_2 Pr \left[\frac{\partial \theta}{\partial \tau} + 4XU \frac{\partial \theta}{\partial X} + (V - YU) \frac{\partial \theta}{\partial Y} \right] = D_4 (1 + \sigma_x^2) \frac{\partial^2 \theta}{\partial Y^2} + \frac{4}{3} Ra \left[3r(1 + r\theta)^2 \left(\frac{\partial \theta}{\partial y} \right)^2 + (1 + r\theta)^3 \frac{\partial^2 \theta}{\partial Y^2} \right], \quad (26)$$

Related to the corresponding boundary and initial conditions are

$$\begin{aligned}
 \tau \leq 0: & \quad U(X, Y, \tau \leq 0) = V(X, Y, \tau \leq 0) = \bar{N}(X, Y, \tau \leq 0) = \theta(X, Y, \tau \leq 0) = 0, \\
 \tau > 0: & \quad \begin{cases} U(X, 0, \tau) = V(X, 0, \tau) = 0, \theta(X, 0, \tau) = 1, \bar{N}(X, 0, \tau) = -\frac{1}{2}(1 + \sigma_x^2) \left(\frac{\partial U}{\partial Y} \right)_{Y=0} \\ U(X, \infty, \tau) \rightarrow 0, \theta(X, \infty, \tau) \rightarrow 0, \bar{N}(X, \infty, \tau) \rightarrow 0. \end{cases} \quad (27)
 \end{aligned}$$

Refer to Appendix A for an explanation of how to get on the final governing system of the physical model, Eqs. (23)-(26), for instance.

The dimensionless local skin friction coefficient, C_f , Nusselt number, Nu_x , and wall couple stress coefficient M_w that are of major importance in materials treatment systems can be expressed as follows:

$$\left. \begin{aligned}
 C_f &= \frac{\tau_w}{\rho U^2} = 2 \sqrt{\frac{4X}{Gr}} \left(D_5 e^{-\beta_1} + \frac{1}{\beta} + \bar{R} e^{-\beta_2} \right) (1 - \sigma_x^2) \left[\frac{\partial U}{\partial X} \right]_{Y=0} + e^{-\beta_2} \left[\frac{\partial U}{\partial Y} + \bar{N} \right]_{Y=0}, \\
 Nu_x &= \frac{\hat{x} q_w}{k_{nf} (T_w - T_\infty)} = \frac{l \left(\frac{\partial T}{\partial n} \right)}{(T_w - T_\infty)} = -X^{3/4} \sqrt{\frac{Gr}{4}} \sqrt{1 + \sigma_x^2} \left[\frac{\partial \theta}{\partial Y} \right]_{Y=0}, \\
 M_w &= \frac{m_w}{l \rho U^2} = \frac{\lambda}{B \sqrt{Gr}} \left[\frac{\partial \bar{N}}{\partial Y} \right]_{Y=0} = \frac{[\Omega]_{Y=0}}{\mu_0 l^2} \left[\frac{\partial \bar{N}}{\partial Y} \right]_{Y=0},
 \end{aligned} \right\} \quad (28)$$



where,

$U = \mu_0 Gr^{1/2} / \rho_f l$: is the characteristic velocity,

$n = (-\hat{\sigma}_x / \sqrt{1 + \hat{\sigma}_x^2}, 1 / \sqrt{1 + \hat{\sigma}_x^2})$: is the unit vector perpendicular to the wavy wall,

$q_w = -k_{nf} (n \cdot \nabla T)_{\hat{y}=\hat{\sigma}(\hat{x})} = -k_{nf} (\partial T / \partial n)_{\hat{y}=\hat{\sigma}(\hat{x})} = -k_{nf} \sqrt{(\partial T / \partial \hat{x})^2 + (\partial T / \partial \hat{y})^2}$: is the wavy wall heat flux,

$m_w = [\Omega(T)(\partial \hat{N} / \partial \hat{x} + \partial \hat{N} / \partial \hat{y})]_{\hat{y}=\hat{\sigma}(\hat{x})}$: is the coupled stress,

$$\lambda = \frac{[\Omega]_{\hat{y}=0}}{\mu_0 j} = \frac{\left(D_5 \mu_0 e^{-\beta_1} + \frac{\kappa_0}{2} e^{-\beta_2} \right)}{\mu_0}$$

$\tau_w = \left[\left(\mu_{nf}(T) + \frac{1}{\beta} + \kappa(T) \right) \left(\frac{\partial \hat{u}}{\partial \hat{y}} + \frac{\partial \hat{v}}{\partial \hat{x}} \right) + \kappa(T) \left(\frac{\partial \hat{u}}{\partial \hat{y}} + \hat{N} \right) \right]_{\hat{y}=\hat{\sigma}(\hat{x})}$: is the shear stress at the wavy wall.

3. Numerical Approach

PDEs (23)-(26) have been used to solve the problem of temporal magnetized non-Newtonian Casson-micropolar nanofluid flow along a vertically heated wavy wall. The implicit Chebyshev pseudo-spectral (ICPS) procedure is an excellent choice for the current study because it provides a highly novel, fast convergence, and optimized procedure (for more details, see Appendix B). This numerical technique is divided into two branches: the first in the spatial domain using the Chebyshev pseudo-spectral method, and the second for the time derivatives using the Crank-Nicolson finite-difference method [63]. Some of the current proposal's results have been compared to publicly available numerical data [65], and good agreement is found, as shown in Fig. 2 at $\beta \rightarrow \infty$ and $\beta_1 = \beta_2 = \bar{R} = Ra = 0.1$. The exciting fit between the current numerical study and previous outcomes allows it to expand the calculated results.

4. Results and Discussion

This numerical study investigated the impact of gold nanoparticles on blood flow near a wavy biological tissue wall using the ICPS technique [66]. The temporal magnetized non-Newtonian Casson-micropolar nanofluid flow over a vertically heated wavy wall was selected as the mathematical model in order to examine certain important properties, such as the fact that the nanofluid flow concerns non-linear thermal radiation, which functions as a heat transfer rate catalyst. Consequently, the following are the numerical results: Table 3 makes clear that the local skin friction for various nanoparticle forms onto the wavy plate reduces with an increase in the variable microrotation viscosity parameter β_2 . Values of the local couple stress and the local Nusselt number for various nanoparticle forms are displayed in Tables 4 and 5 when the variable microrotation viscosity parameter β_2 is present. It has been noted that rising values of drive rising numbers for Nu and M_w results.

Figure 3 depicts the distributions of transient dimensionless axial velocities, $U, -V$, temperature, θ , and microrotation velocity, \bar{N} . Figure 3 depicts how the axial velocities, temperature, and microrotation velocity profiles have changed after nominating times. The velocity curves move away from the wall as time passes until they reach a steady state. Furthermore, the axial velocities increase until the crest and then gradually decrease as the distance from the origin point to the edge increases. Figure 4 also illustrates the impacts of various time step values on couple stress distributions, skin friction, and Nusselt number for nanoparticle column shape at $Pr = 21, \tau = 0.01, \alpha_1 = \alpha_2 = 0.05, \beta_1 = \beta_2 = 0.05, M = B = r = 0.5$, and $\bar{R} = Ra = 0.1$. It is evident that the value of local skin friction increases as the τ parameter increases. Over time, local skin friction likewise attains a steady state at $\tau = 0.03$. While parameter τ increases, the Nusselt number and couple stress distributions for nanoparticle column shape decrease. Furthermore, the thermal boundary layer improves over time for all profiles in Figs. 3 and 4. However, it is clear that as time passes, the efficacy of all profiles decreases, and the unstable situation approaches a steady state. Based on [67], the current numerical approach achieves steady-state in less time than previous studies, such as [52, 65].

Table 3. The variable microrotation viscosity parameter β_2 influences local skin friction for different nanoparticle shapes at $Pr = 21, \tau = 0.01, \alpha_1 = \alpha_2 = 0.05, \beta = \beta_1 = 0.01, M = B = r = 0.5$, and $\bar{R} = Ra = 0.1$.

(a) Column			
X	$\beta_2 = 0.5$	$\beta_2 = 1$	$\beta_2 = 5$
0.051111261	0.306514749	0.306661558	0.306733549
0.439339828	0.379143938	0.379337701	0.379437691
0.75	0.155488082	0.155594965	0.155655603
1.5	0.745670523	0.746024014	0.746195711
2.560660172	0.588209786	0.588510765	0.588666172
3	0.885622179	0.886042462	0.886246631
(b) Tetrahedron			
0.051111261	0.2011585	0.201273214	0.20132365
0.439339828	0.253464335	0.253594862	0.253652556
0.75	0.105442346	0.105469062	0.105476492
1.5	0.486948211	0.487229862	0.487353171
2.560660172	0.393464743	0.393667543	0.393757238
3	0.578481126	0.578816024	0.57896266
(c) Sphere			
0.051111261	1.912425128	1.912425127	1.912425126
0.439339828	1.921700375	1.921700378	1.921700378
0.75	1.928780593	1.92878059	1.928780587
1.5	1.909611797	1.909611797	1.909611796
2.560660172	1.921788198	1.921788187	1.921788178
3	1.910146165	1.910146084	1.910146032



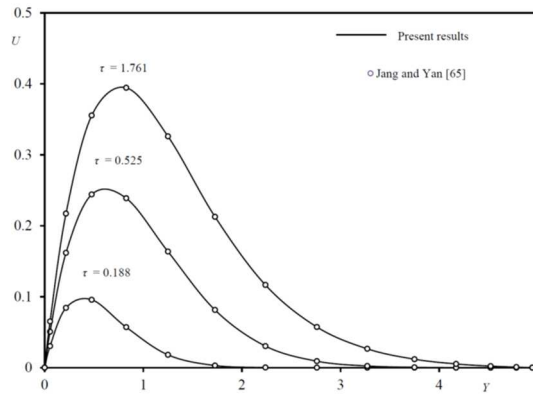


Fig. 2. Transient velocity profile comparison with Jang and Yan [65].

Table 4. The variable microrotation viscosity parameter β_2 influences the local Nusselt number for different nanoparticle shapes at $Pr = 21, \tau = 0.01, \alpha_1 = \alpha_2 = 0.05, \beta = \beta_1 = 0.01, M = B = r = 0.5$, and $\bar{R} = Ra = 0.1$.

(a) Column			
X	$\beta_2 = 0.5$	$\beta_2 = 1$	$\beta_2 = 5$
0.051111261	1.912425126	1.912425127	1.912425128
0.439339828	1.921700378	1.921700378	1.921700375
0.75	1.928780587	1.92878059	1.928780593
1.5	1.909611796	1.909611797	1.909611797
1.888228568	1.921221117	1.921221127	1.921221141
2.560660172	1.921788178	1.921788187	1.921788198
3	1.910146032	1.910146084	1.910146165
(b) Tetrahedron			
X	$\beta_2 = 0.5$	$\beta_2 = 1$	$\beta_2 = 5$
0.051111261	1.857190713	1.857190714	1.857190715
0.439339828	1.876334269	1.876334269	1.876334268
0.75	1.891014417	1.891014419	1.891014422
1.5	1.851432979	1.85143298	1.851432979
2.560660172	1.876429046	1.876429053	1.876429062
3	1.85200701	1.85200705	1.852007115
(c) Sphere			
X	$\beta_2 = 0.5$	$\beta_2 = 1$	$\beta_2 = 5$
0.051111261	0.618770892	0.618770892	0.618770892
0.439339828	0.690263531	0.690263531	0.690263531
0.75	0.764831382	0.764831383	0.764831384
1.5	0.601080349	0.601080349	0.601080349
2.560660172	0.69026458	0.69026458	0.69026458
3	0.601107528	0.601107529	0.601107529

Table 5. The variable microrotation viscosity parameter β_2 influences the local couple stress for different nanoparticle shapes at $Pr = 21, \tau = 0.01, \alpha_1 = \alpha_2 = 0.05, \beta = \beta_1 = 0.01, M = B = r = 0.5$, and $\bar{R} = Ra = 0.1$.

(a) Column			
X	$\beta_2 = 0.5$	$\beta_2 = 1$	$\beta_2 = 5$
0.051111261	0.000191442	0.000191492	0.000191565
0.439339828	0.000253269	0.000253331	0.000253422
0.75	0.000329229	0.000329306	0.000329428
1.5	0.000177793	0.000177838	0.0001779
2.560660172	0.000253147	0.000253209	0.0002533
3	0.000177759	0.000177804	0.000177864
(b) Tetrahedron			
X	$\beta_2 = 0.5$	$\beta_2 = 1$	$\beta_2 = 5$
0.051111261	0.000196096	0.00019613	0.000196182
0.439339828	0.000261395	0.000261438	0.000261504
0.75	0.000342561	0.000342616	0.000342705
1.5	0.000181735	0.000181766	0.00018181
2.560660172	0.000261167	0.00026121	0.000261275
3	0.000181681	0.000181711	0.000181754
(c) Sphere			
X	$\beta_2 = 0.5$	$\beta_2 = 1$	$\beta_2 = 5$
0.051111261	0.000269971	0.000269998	0.000270037
0.439339828	0.000281414	0.000281439	0.000281475
0.75	0.0002988	0.000298825	0.000298863
1.5	0.00020452	0.000204538	0.000204564
2.560660172	0.000219559	0.000219576	0.000219603
3	0.000185481	0.000185494	0.000185509

Figures 5 and 6 show the consequences of several different nanoparticle shapes -sphere, tetrahedron, and column- on the spreads of Nusselt numbers, heat, microrotation, skin the friction, and motion at $Pr = 21, \beta_1 = 0.01, \tau = 0.01, \alpha_1 = \alpha_2 = 0.05, \beta = \beta_2 = 0.01, M = B = r = 0.5$, and $\bar{R} = Ra = 0.1$. As seen in Figs. 5(a), 5(b), and 5(c), the microrotation changes decrease as the velocity and temperature distributions increase. The spheres have a substantial effect on the temperature and velocity ranges, as Figs. 5(a)



and 5(b) demonstrate. Radiation causes conduction to become more dominant over radiation, which lowers the buoyancy force and thickness of the thermal boundary layer. Further, because of their low viscosity, sphere-shaped nanoparticles have the highest temperature and velocity. Nonetheless, the microrotation velocity distributions for the column's nanoparticle shape are the best when compared to other shapes [28]. Similarly, as Fig. 6(a) shows, column-shaped nanoparticles have the most influence on skin friction distributions of all other nanoparticle shapes, while column-shaped nanoparticles have the greatest influence on skin friction distributions (see Fig. 6(b)). Figure 7 depicts the effects of β_1 on velocity, skin friction, and Nusselt number distributions for various nanoparticle shapes at $Pr = 21, \tau = 0.01, \alpha_1 = \alpha_2 = 0.05, \beta = \beta_2 = 0.01, M = B = r = 0.5,$ and $\bar{R} = Ra = 0.1$. It should be noted that the current study is primarily concerned with the role of viscosity as a variable property.

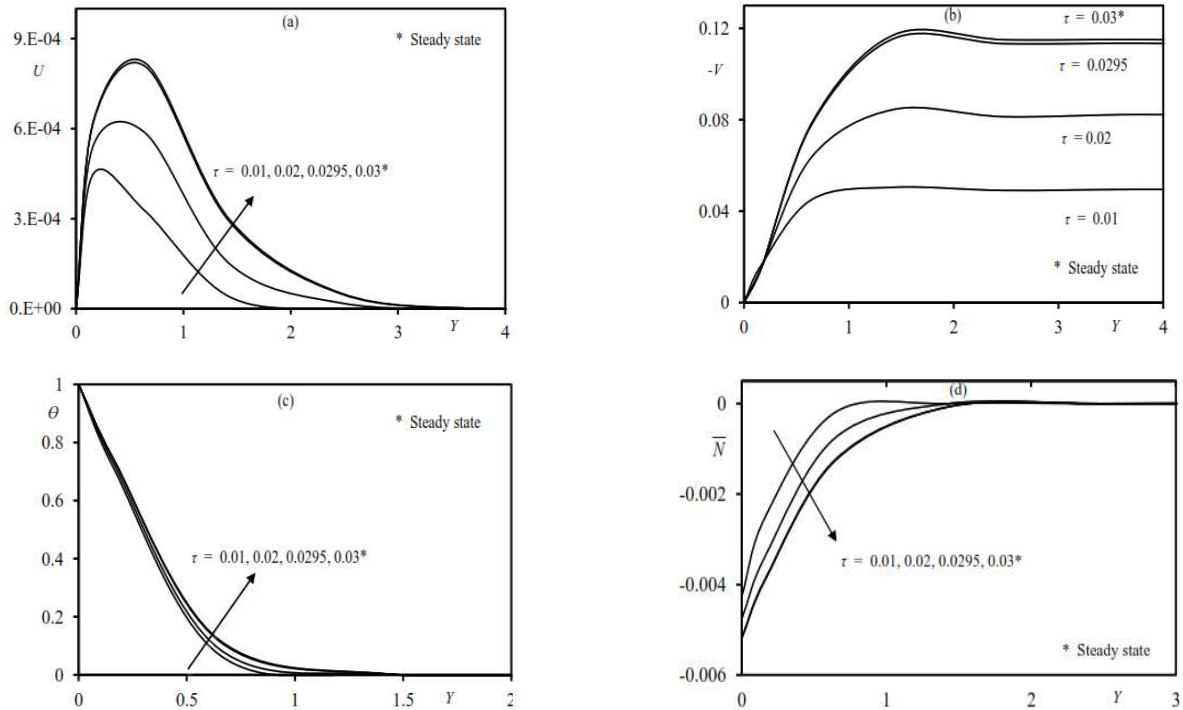


Fig. 3. The effects of parameter τ on nanoparticle column shape velocities, temperature, and microrotation velocity distributions.

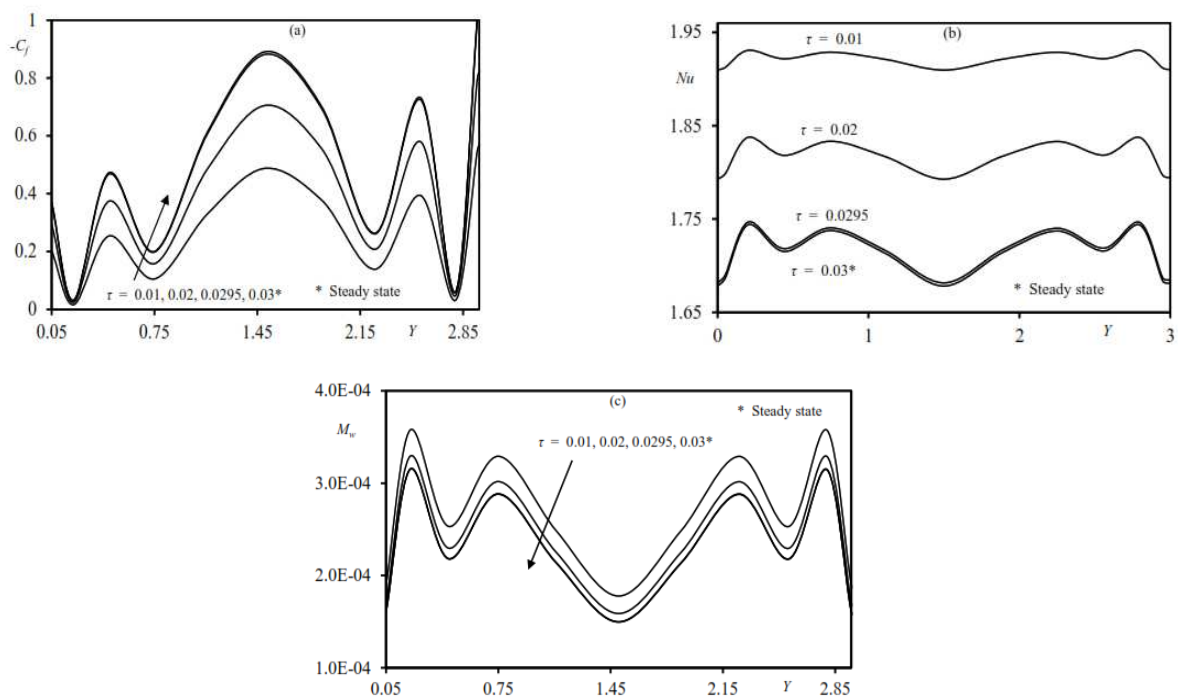


Fig. 4. The effects of parameter τ on nanoparticle column shape skin friction, Nusselt number, and couple stress distributions.



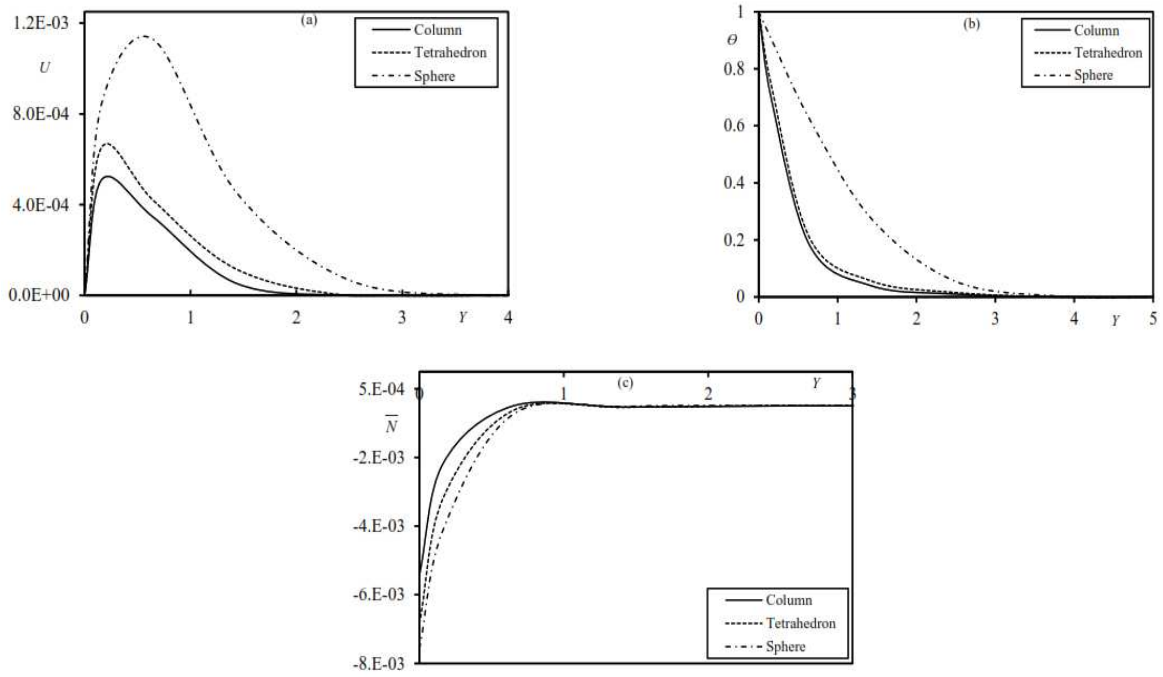


Fig. 5. The effects of different nanoparticle shapes on velocities, temperature, and microrotation velocity distributions.

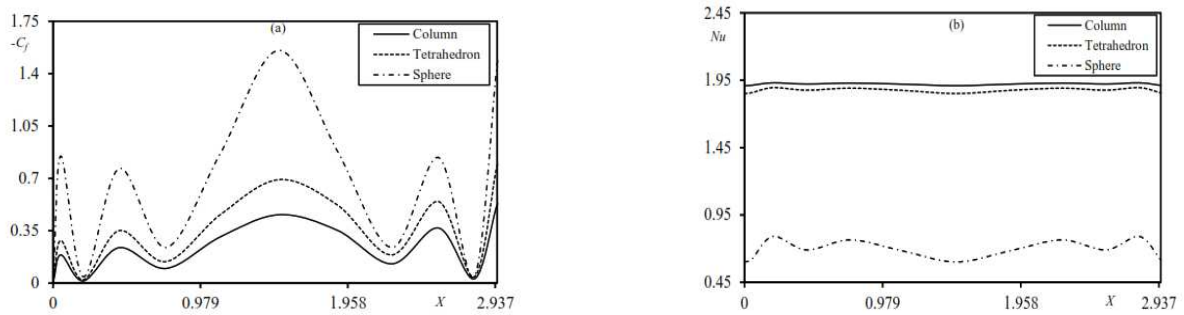


Fig. 6. The effects of different nanoparticle shapes on skin friction and Nusselt number distributions.

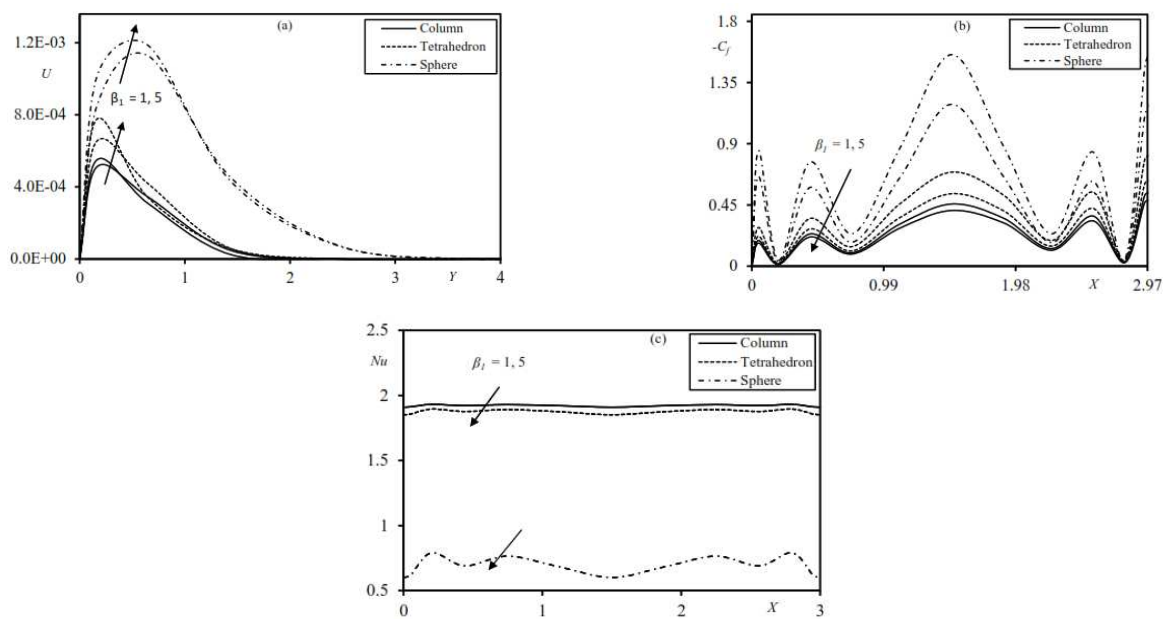


Fig. 7. The effects of β_1 for different nanoparticle shapes on velocity, skin friction and Nusselt number distributions.



Examining the numerical results in Fig. 7 reveals this function's characteristics. The velocity curves have two stages, as seen in Fig. 7(a): initially, they achieve the boundary condition; subsequently, they progressively increase the thermal boundary layer. Moreover, the velocity curves rise to the crest and then progressively decrease as the value of Y increases. Additionally, sphere-shaped nanoparticles have the highest velocity due to their low viscosity. In contrast, as the number of nanoparticles grows in β_1 , the skin friction and Nusselt number distributions in Figs. 7(b) and 7(c) decrease. As shown in Fig. 7(b), the highest value of the local skin friction coefficients is at $X \approx 1.5$, while the lowest value is at $X \approx 0.25$. Additionally, the nanoparticles with a column shape have the highest Nusselt number. The flow can go comparatively deeper at low β_1 values. After that, the depth of the Nusselt number profiles increases with an increase in β_1 . Figure 8 depicts the effects of α_1 and α_2 on skin friction and Nusselt number distributions for various nanoparticle shapes at $Pr = 21, \tau = 0.01, \beta_1 = 1, \beta = \beta_2 = 0.01, M = B = r = 0.5$, and $\bar{R} = Ra = 0.1$. Figures 8(a) and (b) show the implications of both of the surface amplitude parameters α_1 and α_2 with the local skin friction and Nusselt number at constant state distributions. Figures 8(a) through 8(b) demonstrate how local skin friction is increased when α_1 and α_2 values are increased while Nusselt number distributions are decreased. Unless stated otherwise, the local Nusselt number can be decreased owing to the amplitude wavy wall parameter. The causes of declines in heat transfer rate are buoyancy and centrifugal forces. Moreover, column-shaped nanoparticles exhibit the largest Nusselt number distributions as the α_1 and α_2 values increase. It is physically seen that the local Nusselt number gradually drops with time. The early phases of the step increase in wall temperature and concentration are characterized by incredibly thin thermal and concentration boundary layers. There are noticeable temperature differences on the surface as a result. Because of this, there is rapid heat transfer, as indicated by the high Nusselt number. With time, the temperature and concentration boundary layer thicknesses, along with the free convection effect, become more noticeable. Consequently, a decrease in the local Nusselt number results in a decrease in the rate of heat transmission.

Figures 9 and 10 represent the effects of M on temperature, skin friction, Nusselt number, and couple stress distributions at $Pr = 21, \tau = 0.01, \alpha_1 = \alpha_2 = 0.05, \beta_1 = 1, \beta = \beta_2 = 0.01, M = B = r = 0.5$, and $\bar{R} = Ra = 0.1$. Moreover, a resistive Lorentz force is created when a magnetic field is applied to the nanofluid, slowing the flow of the fluid. As seen in Figs. 9 and 10, a transverse magnetic field applied to an electrically conducting fluid increases the resistive force, causing the fluid to flow more slowly. Consequently, the change in axial velocity at different time steps is inversely proportional to the magnetic field parameter. Increasing the magnetic parameter, as Fig. 9(a) illustrates, raises the temperature function, and the nanoparticles with a sphere shape have the highest temperature. On the other side, Figs. 9(b), 9(c), 10(a), and 10(b) illustrate decreased skin friction, Nusselt number, and couple stress distributions.

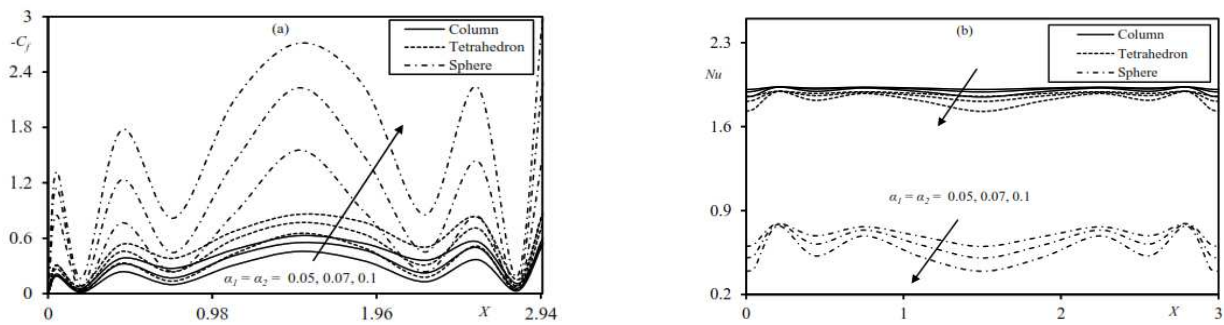


Fig. 8. The effects of α_1 and α_2 for different nanoparticle shapes on skin friction and Nusselt number distributions.

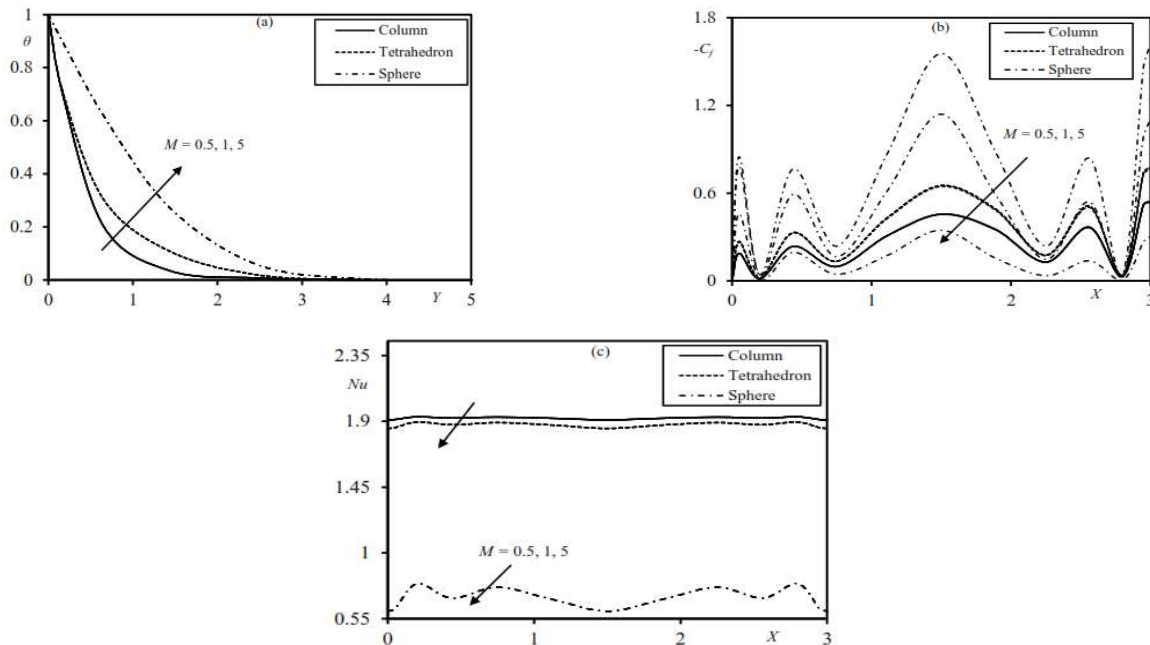


Fig. 9. The effects of M for different nanoparticle shapes on temperature, skin friction and Nusselt number distributions.



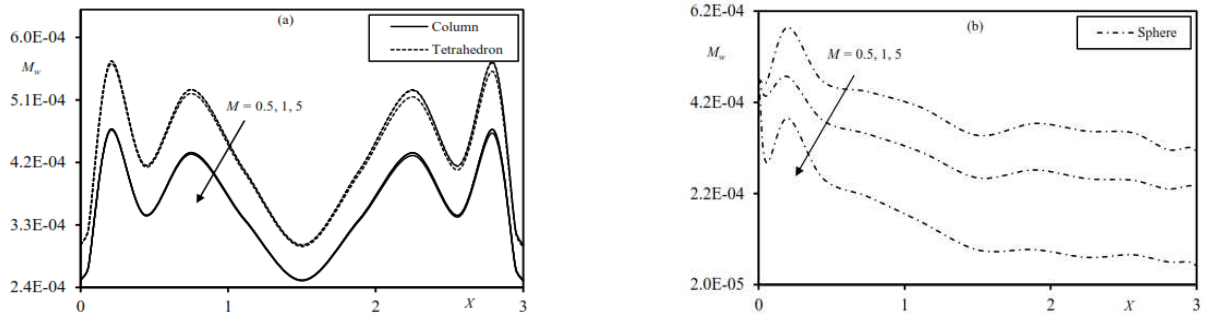


Fig. 10. The effects of M for different nanoparticle shapes on couple stress distributions.

5. Conclusion

In the current study, the effect of introducing gold nanoparticles on blood flow near a wavy biological tissue wall that forms during cancer treatment was examined. It was also assessed what impact the additional gold nanoparticle shapes would have. This objective was investigated using a mathematical model of an unstable magneto-non-Newtonian Casson-micropolar flow of nanofluid across a vertically heated wavy surface. Two variables associated with blood temperature that have been identified are microrotation and nanofluid viscosity. When some of the outcomes of the proposed approach are compared with numerical data that is readily available to the public [65], good agreement is discovered, as Fig. 2 illustrates. Applications of interest include the design of heat exchangers and chemical processing equipment, the formation and dispersal of fog, temperature and moisture distributions over agricultural fields, environmental pollution, and thermoprotection systems. These applications involve the combined transfer of mass and heat through natural convection. Plotting blood flow as a function of several physical characteristics has produced the following results, which are highlighted:

- As the unstable state gives way to the steady state, the efficiency of all distributions steadily vanishes.
- As the values of the viscosity-temperature variation parameter grow, the transient local skin friction coefficient and transient local Nusselt number fall.
- While sphere-shaped nanoparticles have a significant effect on temperature profile change, column-shaped nanoparticles have little effect.
- Columnar-shaped nanoparticles govern the rate of heat transfer, whereas spherically-shaped nanoparticles serve a lesser purpose.
- The effects of temperature, velocity, and local skin friction profiles against angular velocity and heat transmission are antagonistic for column and sphere-shaped nanoparticles.
- The thickness of the resultant thermal boundary layer was decreased by raising the variable viscosity parameter.
- Skin friction, Nusselt number, and couple stress distributions decreased as magnetic field values increased, but temperature fields strengthened.
- The local skin friction rises and the local Nusselt number falls as the values of the two surface amplitude parameters, α_1 and α_2 , grow.

APPENDIX A

To show the details of obtaining equation (26), we start from equation (6):

$$(\rho C_p)_{nf} \left(\frac{\partial T}{\partial t} + \hat{u} \frac{\partial T}{\partial \hat{x}} + \hat{v} \frac{\partial T}{\partial \hat{y}} \right) = k_{nf} \left(\frac{\partial^2 T}{\partial \hat{x}^2} + \frac{\partial^2 T}{\partial \hat{y}^2} \right) - \frac{\partial q_r}{\partial \hat{y}}. \tag{6}$$

And using equations (7)-(11) as follows:

$$\left(\frac{\mu_0 Gr^{\frac{1}{2}}}{\rho_f l^2} (T_w - T_\infty) \frac{\partial \theta}{\partial t} + \frac{\mu_0 Gr^{\frac{1}{2}}}{\rho_f l^2} (T_w - T_\infty) u \frac{\partial \theta}{\partial x} - \frac{\mu_0 Gr^{\frac{3}{4}}}{\rho_f l^2} (T_w - T_\infty) \sigma_x u \frac{\partial \theta}{\partial y} + \frac{\mu_0 Gr^{\frac{1}{2}}}{\rho_f l^2} (T_w - T_\infty) v \frac{\partial \theta}{\partial y} + \frac{\mu_0 Gr^{\frac{3}{4}}}{\rho_f l^2} (T_w - T_\infty) \sigma_x v \frac{\partial \theta}{\partial y} \right) = \frac{k_{nf}}{(\rho C_p)_{nf}} \left((1 + \sigma_x^2) \frac{\partial^2 \theta}{\partial y^2} \right) - \frac{1}{(\rho C_p)_{nf}} \left[\frac{\partial q_r}{\partial y} Gr^{\frac{1}{4}} \right]. \tag{*}$$

After that, we divide the above equation (*) on the coefficient $(\mu_0 Gr^{1/2} / \rho_f l^2)(T_w - T_\infty)$ of $\partial \theta / \partial t$, and then we get equation (19) as follows:

$$D_2 Pr \left[\frac{\partial \theta}{\partial t} + u \frac{\partial \theta}{\partial x} + v \frac{\partial \theta}{\partial y} \right] = D_4 (1 + \sigma_x^2) \frac{\partial^2 \theta}{\partial y^2} + \frac{4}{3} Ra \left[3r(1 + r\theta)^2 \left(\frac{\partial \theta}{\partial y} \right)^2 + (1 + r\theta)^3 \frac{\partial^2 \theta}{\partial y^2} \right]. \tag{19}$$

By using the transformation (22) to convert the current complex wavy wall to another flat plate, as follows:

$$\frac{\partial \theta}{\partial t} = \frac{\partial \theta}{\partial \tau} \cdot \frac{\partial \tau}{\partial t} = (4X)^{-\frac{1}{2}} \frac{\partial \theta}{\partial \tau}, \tag{**}$$



$$u \frac{\partial \theta}{\partial X} = (4X)^{\frac{1}{2}} U \left(\frac{\partial \theta}{\partial X} \cdot \frac{\partial X}{\partial x} + \frac{\partial \theta}{\partial Y} \cdot \frac{\partial Y}{\partial x} \right) = (4X)^{\frac{1}{2}} U \frac{\partial \theta}{\partial X} - (4X)^{-\frac{3}{4}} y U \frac{\partial \theta}{\partial Y},$$

$$v \frac{\partial \theta}{\partial y} = (4X)^{\frac{1}{4}} V \left(\frac{\partial \theta}{\partial Y} \cdot \frac{\partial Y}{\partial y} \right) = (4X)^{\frac{1}{2}} V \frac{\partial \theta}{\partial Y},$$

$$\frac{\partial^2 \theta}{\partial y^2} = \frac{\partial}{\partial Y} \left(\frac{\partial \theta}{\partial Y} \cdot \frac{\partial Y}{\partial y} \right) \cdot \frac{\partial Y}{\partial y} = (4X)^{-\frac{1}{2}} \frac{\partial^2 \theta}{\partial Y^2},$$

$$\left(\frac{\partial \theta}{\partial y} \right)^2 = (4X)^{-\frac{1}{2}} \left(\frac{\partial \theta}{\partial Y} \right)^2.$$

Therefore, using equations (**), equation (19) converts to the following equation (26):

$$D_2 Pr \left[\frac{\partial \theta}{\partial \tau} + 4XU \frac{\partial \theta}{\partial X} + (V - YU) \frac{\partial \theta}{\partial Y} \right] = D_4 (1 + \sigma_x^2) \frac{\partial^2 \theta}{\partial Y^2} + \frac{4}{3} Ra \left[3r(1 + r\theta)^2 \left(\frac{\partial \theta}{\partial y} \right)^2 + (1 + r\theta)^3 \frac{\partial^2 \theta}{\partial Y^2} \right], \tag{26}$$

APPENDIX B

We express the assumptions and limitations of our methods as follows [67]:

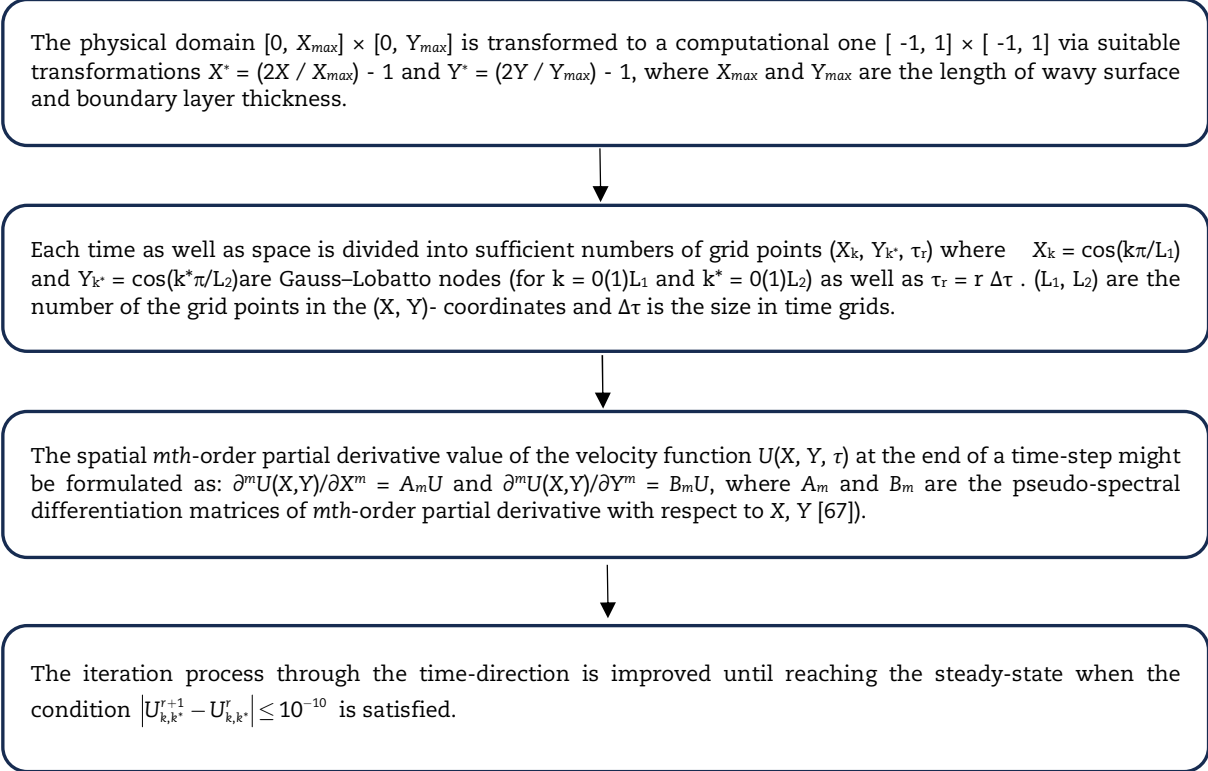


Fig. 11. The flowchart for highlighted numerical approach.

Author Contributions

Ji-Huan He supervised and administered the project; Nasser S. Elgazery conceptualized the physical issue and made a mathematical suggestion; Nader Y. Abd Elazem created a mathematical model, applied the numerical approach, plotted the data, analyzed the numerical outcomes. The manuscript was written through the contribution of all authors. All authors contributed to the writing of the manuscript. The final version of the article was reviewed by all authors, who also gave their approval.

Acknowledgments

The reviewers' insightful observations, supportive remarks, and helpful recommendations to enhance the original article are all greatly appreciated by the authors.



Conflict of Interest

Regarding the research, writing, and/or publication of this work, the authors declared that there were no potential conflicts of interest.

Funding

The authors received no financial support of the authorship, work, and/or publication of the current manuscript.

Data Availability Statements

The datasets generated and/or analyzed during the current study are available from the corresponding author on reasonable request.

Nomenclature

Appellations Roman Symbols

\hat{a}_1, \hat{a}_2	The characteristic amplitude value of wavy wall
B	Dimensionless parameter
B_0^2	The magnetic field
Cf	The local skin friction coefficient
C_p	The specific heat at constant pressure
g	The acceleration due to gravity vector
Gr	The Grashof number
j	The constant microinertia density
k_{nf}	The thermal conductivity
l	Characteristic length
M	Magnetic field parameter
M_w	Wall couple stress coefficient
n	The unit vector perpendicular to the wavy wall
Nu_x	Nusselt number coefficient
\hat{N}	The microrotation velocity
\hat{p}	The pressure
Pr	The Prandtl number
q_r	The non-linear thermal radiative heat flux
\bar{R}	Dimensionless microrotation parameter
r	Relative temperature difference within blood flow
Ra	Non-linear thermal radiation parameter
\hat{t}	The time
T	The nanofluid temperature
\hat{u}, \hat{v}	Nanofluid velocities in the directions (\hat{x}, \hat{y}) along and perpendicular to the tangent of the wavy wall

Greek Symbols

β	Upper limit apparent nanofluid viscosity coefficient parameter
β_T	The thermal expansion coefficient
δ	Stefan-Boltzman constant
θ	Dimensionless temperature
κ	The variable microrotation
μ_0	Constant viscosity
μ_{nf}	The nanofluid viscosity
$\nu_0 = \mu_0 / \rho_f$	The blood kinematic viscosity
ρ_{nf}	The density of the nanofluid
$\hat{\sigma}(\hat{x})$	The wavy wall
σ_{nf}	The electrical conductivity of the nanofluid
Ω	Spin gradient viscosities
Δ	Mean absorption coefficient

Subscripts

f	Base fluid (blood)
nf	Nanofluid
s	Nano-solid-particles (gold)



w	Condition on the wavy wall
∞	Far field
Superscript	
\sim	Nondimensional quantity


References


- [1] Eringen, A.C., Theory of micropolar fluids, *Journal of Mathematics and Mechanics*, 16, 1966, 1–18.
- [2] Eringen, A.C., *Mechanics of micromorphic continua*, in *Mechanics of generalized continua*, Springer, 1968.
- [3] Eringen, A.C., Theory of thermomicrofluids, *Journal of Mathematical analysis and Applications*, 38(2), 1972, 480–496.
- [4] Elgazery, N.S., Numerical simulation for biviscosity fluid flow through a porous medium under the effects of variable properties, *Special Topics and Reviews in Porous Media*, 3(1), 2012, 1–11.
- [5] Chaturani, P., Upadhya, V.S., On micropolar fluid model for blood flow through narrow tubes, *Biorheology*, 16(6), 1979, 419–428.
- [6] Mekheimer, K.S., El Kot, M.A., The micropolar fluid model for blood flow through a tapered artery with a stenosis, *Acta Mechanica Sinica*, 24(6), 2008, 637–644.
- [7] Abdullah, I., Amin, N., A micropolar fluid model of blood flow through a tapered artery with a stenosis, *Mathematical Methods in the Applied Sciences*, 33(16), 2010, 1910–1923.
- [8] Ellahi, R., Rahman, S.U., Gulzar, M.M., Nadeem, S., Vafai, K., A mathematical study of non-Newtonian micropolar fluid in arterial blood flow through composite stenosis, *Applied Mathematics & Information Sciences*, 8(4), 2014, 1567.
- [9] Ellahi, R., Rahman, S.U., Nadeem, S., Akbar, N.S., Influence of heat and mass transfer on micropolar fluid of blood flow through a tapered stenosed arteries with permeable walls, *Journal of Computational and Theoretical Nanoscience*, 11(4), 2014, 1156–1163.
- [10] Mekheimer, K.S., Elnaqeeb, T., El Kot, M.A., Alghamdi, F., Simultaneous effect of magnetic field and metallic nanoparticles on a micropolar fluid through an overlapping stenotic artery: Blood flow model, *Physics Essays*, 29(2), 2016, 272–283.
- [11] Muthu, P., Rathish Kumar, B.V., Chandra, P., A study of micropolar fluid in an annular tube with application to blood flow, *Journal of Mechanics in Medicine and Biology*, 8(4), 2008, 561–576.
- [12] Misra, J.C., Chandra, S., Shit, G.C., Kundu, P.K., Electroosmotic oscillatory flow of micropolar fluid in microchannels: application to dynamics of blood flow in microfluidic devices, *Applied Mathematics and Mechanics*, 35(6), 2014, 749–766.
- [13] Asha, S.K., Deepa, C.K., Entropy generation for peristaltic blood flow of a magneto-micropolar fluid with thermal radiation in a tapered asymmetric channel, *Results in Engineering*, 3, 2019, 100024.
- [14] Karvelas, E., Sofiadis, G., Papathanasiou, T., Sarris, I., Effect of micropolar fluid properties on the blood flow in a human carotid model, *Fluids*, 5(3), 2020, 125.
- [15] Chaturani, P., Samy, R.P., Pulsatile flow of Casson's fluid through stenosed arteries with applications to blood flow, *Biorheology*, 23(5), 1986, 499–511.
- [16] Chaturani, P., Palanisamy, V., Casson fluid model for pulsatile flow of blood under periodic body acceleration, *Biorheology*, 27(5), 1990, 619–630.
- [17] Srivastava, V.P., Saxena, M., Two-layered model of Casson fluid flow through stenotic blood vessels: applications to the cardiovascular system, *Journal of Biomechanics*, 27(7), 1994, 921–928.
- [18] Venkatesan, J., Sankar, D.S., Hemalatha, K., Yatim, Y., Mathematical analysis of Casson fluid model for blood rheology in stenosed narrow arteries, *Journal of Applied Mathematics*, 2013, 2013, 583809.
- [19] Ali, F., Sheikh, N.A., Khan, I., Saqib, M., Magnetic field effect on blood flow of Casson fluid in axisymmetric cylindrical tube: A fractional model, *Journal of Magnetism and Magnetic*, 423, 2017, 327–336.
- [20] Khan, M.W.S., Ali, N., Theoretical analysis of thermal entrance problem for blood flow: an extension of classical Graetz problem for Casson fluid model using generalized orthogonality relations, *International Communications in Heat and Mass*, 109, 2019, 104314.
- [21] Kumar, M., Mondal, P.K., Bejan's flow visualization of buoyancy-driven flow of a hydromagnetic Casson fluid from an isothermal wavy surface, *Physics of Fluids*, 33(9), 2021, 93113.
- [22] Iqbal, Z., Mehmood, R., Azhar, E., Mehmood, Z., Impact of inclined magnetic field on micropolar Casson fluid using Keller box algorithm, *The European Physical Journal Plus*, 132(4), 2017, 1–13.
- [23] Mehmood, Z., Mehmood, R., Iqbal, Z., Numerical investigation of micropolar Casson fluid over a stretching sheet with internal heating, *Communications in Theoretical Physics*, 67(4), 2017, 443.
- [24] Ali, A., Umar, M., Bukhari, Z., Abbas, Z., Pulsating flow of a micropolar-Casson fluid through a constricted channel influenced by a magnetic field and Darcian porous medium: A numerical study, *Results in Physics*, 19, 2020, 103544.
- [25] Elelmy, A.F., Elgazery, N.S., Ellahi, R., Blood flow of MHD non-Newtonian nanofluid with heat transfer and slip effects: Application of bacterial growth in heart valve, *International Journal of Numerical Methods for Heat & Fluid Flow*, 30(11), 2020, 4883–4908.
- [26] Amjad, M., Zehra, I., Nadeem, S., Abbas, N., Saleem, A., Issakhov, A., Influence of Lorentz force and induced magnetic field effects on Casson micropolar nanofluid flow over a permeable curved stretching/shrinking surface under the stagnation region, *Surfaces and Interfaces*, 21, 2020, 100766.
- [27] Chu, Y.-M., Khan, U., Shafiq, A., Zaib, A., Numerical simulations of time-dependent micro-rotation blood flow induced by a curved moving surface through conduction of gold particles with non-uniform heat sink/source, *Arabian Journal for Science and Engineering*, 46(3), 2021, 2413–2427.
- [28] Rashid, U., Abdeljawad, T., Liang, H., Iqbal, A., Abbas, M., Siddiqui, M.J., The shape effect of gold nanoparticles on squeezing nanofluid flow and heat transfer between parallel plates, *Mathematical Problems in Engineering*, 2020, 2020, 9584854.
- [29] Mekheimer, K.S., Hasona, W.M., Abo-Elkhair, R.E., Zaher, A.Z., Peristaltic blood flow with gold nanoparticles as a third grade nanofluid in catheter: Application of cancer therapy, *Physics Letters A*, 382(2-3), 2018, 85–93.
- [30] Eldabe, N.T., Moatimid, G.M., El-Shehpiy, A.A., Aballah, N.F., Peristaltic blood flow with gold nanoparticles on a Carreau nanofluid through a non-darcian porous medium, *Journal of Biomaterials and Nanobiotechnology*, 9(4), 2018, 290–306.
- [31] Elnaqeeb, T., Shah, N.A., Mekheimer, K.S., Hemodynamic characteristics of gold nanoparticle blood flow through a tapered stenosed vessel with variable nanofluid viscosity, *Bionanoscience*, 9(2), 2019, 245–255.
- [32] Mekheimer, K.S., Abo-Elkhair, R.E., Moawad, A.M.A., Electrothermal transport via gold nanoparticles as antimicrobials of blood flow through an electro-osmosis artery with overlapping stenosis, *International Journal of Fluid Mechanics Research*, 47(2), 2020, 135–152.
- [33] Iftikhar, N., Sadaf, H., Rehman, A., Consequences of gold nanoparticles of MHD blood flow in a wavy tube with wall properties, *Waves in Random and Complex Media*, 2022, 1–17.
- [34] He, J.H., Abd Elazem, N.Y., The carbon nanotube-embedded boundary layer theory for energy harvesting, *Facta Universitatis, Series: Mechanical Engineering*, 20(2), 2022, 211–235.
- [35] Mousavi, S.M., Rostami, M.N., Yousefi, M., Dinarvand, S., Dual solutions for MHD flow of a water-based TiO₂-Cu hybrid nanofluid over a continuously moving thin needle in presence of thermal radiation, *Reports in Mechanical Engineering*, 2(1), 2021, 31–40.
- [36] Al-Griffi, T.A.J., Al-Saif, A.S.J., Analytical Investigations for the Joint Impacts of Electro-osmotic and Some Relevant Parameters to Blood Flow in Mildly Stenosis Artery, *Journal of Applied and Computational Mechanics*, 9(1), 2023, 274–293.
- [37] Munafa, C.F., Rogolino, P., Analysis of a Hyperbolic Heat Transfer Model in Blood-perfused Biological Tissues with Laser Heating, *Journal of Applied and Computational Mechanics*, 8(4), 2022, 1398–1406.
- [38] Nadeem, S., Amin, A., Abbas, N., Saleem, A., Alharbi, F.M., Hussain, A., Issakhov, A., Effects of heat and mass transfer on stagnation point flow of micropolar Maxwell fluid over Riga plate, *Scientia Iranica*, 28(6), 2021, 3753–3766.
- [39] Madhura, K.R., Babitha, Numerical study on magnetohydrodynamics micropolar Carreau nanofluid with Brownian motion and thermophoresis effect, *International Journal of Modelling and Simulation*, 2023, 1–14, <https://doi.org/10.1080/02286203.2023.2234240>.
- [40] Makinde, O.D., Reddy, M.G., MHD peristaltic slip ow of Casson uid and heat transfer in channel filed with a porous medium, *Scientia Iranica B*, 26(4), 2019, 2342–2355.




- [41] Truskey, G.A., Yuan, F., Katz, D.F., *Transport phenomena in biological systems*, Pearson Prentice Hall, Upper Saddle River, 2004.
- [42] Rashad, A.M., Nabwey, H.A., Gyrotactic mixed bioconvection flow of a nanofluid past a circular cylinder with convective boundary condition, *Journal of the Taiwan Institute of Chemical Engineers*, 99, 2019, 9-17.
- [43] Elgazery, N.S., Elelmy, A.F., Bobescu, E., Ellahi, R., How do artificial bacteria behave in magnetized nanofluid with variable thermal conductivity: Application of tumor reduction and cancer cells destruction, *International Journal of Numerical Methods for Heat & Fluid Flow*, 32(9), 2022, 2982-3006.
- [44] Mekheimer, K.S., Hasona, W.M., Abo-Elkhair, R.E., Zaher, A.Z., Peristaltic blood flow with gold nanoparticles as a third grade nanofluid in catheter: Application of cancer therapy, *Physics Letters A*, 382(2-3), 2018, 85-93.
- [45] Bhatti, M.M., Zeeshan, A., Ellahi, R. Endoscope analysis on peristaltic blood flow of Sisko fluid with Titanium magneto-nanoparticles, *Computers in Biology and Medicine*, 78, 2016, 29-41.
- [46] Abbasi, A., Farooq, W., Tag-ElDin, E.S.M., Khan, S.U., Khan, M.I., Guedri, K., Galal, A.M., Heat transport exploration for hybrid nanoparticle (Cu, Fe₃O₄)—Based blood flow via tapered complex wavy curved channel with slip features, *Micromachines*, 13(9), 2022, 1415.
- [47] Zhang, L., Bhatti, M.M., Michaelides, E.E., Entropy generation in magnetized blood flow through a finite wavy channel under slip conditions, *Journal of Non-Equilibrium Thermodynamics*, 45(4), 2020, 419-429.
- [48] Majee, S., Maiti, S., Shit, G.C., Maiti, D.K., Spatio-temporal evolution of magnetohydrodynamic blood flow and heat dynamics through a porous medium in a wavy-walled artery, *Computers in Biology and Medicine*, 135, 2021, 104595.
- [49] Shami, S., Sajid, M., Javed, T., Impact of complex wavy surface on natural convection flow in micropolar fluid, *Numerical Methods for Partial Differential Equations*, 38(3), 2022, 591-607.
- [50] He, J.-H., Elgazery, N.S., Abd Elazem, N.Y., Magneto-radiative gas near an unsmooth boundary with variable temperature, *International Journal of Numerical Methods for Heat & Fluid Flow*, 33(2), 2023, 545-569.
- [51] Hady, F.M., Mahdy, A., Mohamed, R.A., Ahmed, S.E., Abo-zaid, O.A., Unsteady natural convection flow of a dusty non-Newtonian Casson fluid along a vertical wavy plate: numerical approach, *Journal of the Brazilian Society of Mechanical Sciences and Engineering*, 41(11), 2019, 1-20.
- [52] Cheng-Ping, C., Huann-Ming, C., Transient analysis of natural convection along a vertical wavy surface in micropolar fluids, *International Journal of Engineering Science*, 32(1), 1994, 19-33.
- [53] Abd Elazem, N.Y., Elgazery, N.S., Unsteady radiative nanofluid flow near a vertical heated wavy surface with temperature-dependent viscosity, *Chinese Journal of Physics*, 74, 2021, 38-52.
- [54] Elgazery, N.S., CPSM simulation of the variable properties' role in MHD non-Newtonian micropolar nanofluid flow over a stretching porous sheet (flow filtration), *Arabian Journal for Science and Engineering*, 46(8), 2021, 7661-7680.
- [55] <https://cetinkaraca.com/wp-content/uploads/2021/03/yemek-borusu-kanseri-risk-faktorleri.jpg>.
- [56] Elgazery, N.S., Elelmy, A.F., Multiple solutions for non-Newtonian nanofluid flow over a stretching sheet with nonlinear thermal radiation: Application in transdermal drug delivery, *Pramana - Journal of Physics*, 94, 2020, 68.
- [57] Chen, C.K., Yang, Y.T., Chang, K.H., The effect of thermal radiation on entropy generation due to micro-polar fluid flow along a wavy surface, *Entropy*, 13(9), 2011, 1595-1610.
- [58] Elgazery, N.S., Flow of non-Newtonian magneto-fluid with gold and alumina nanoparticles through a non-Darcian porous medium, *Journal of the Egyptian Mathematical Society*, 27(1), 2019, 1-25.
- [59] Elgazery, N.S., Nanofluids flow over a permeable unsteady stretching surface with non-uniform heat source/sink in the presence of inclined magnetic field, *Journal of the Egyptian Mathematical Society*, 27(1), 2019, 1-26.
- [60] Khan, A.A., Bukhari, S.R., Marin, M., Ellahi, R., Effects of chemical reaction on third-grade MHD fluid flow under the influence of heat and mass transfer with variable reactive index, *Heat Transfer Research*, 50(11), 2019, 1061-1080.
- [61] Hossain, M.A., Kabir, S., Rees, D.A.S., Natural convection of fluid with variable viscosity from a heated vertical wavy surface, *Zeitschrift für Angewandte Mathematik und Physik*, 53(1), 2002, 48-57.
- [62] Yao, L.S., Natural convection along a vertical wavy surface, *Journal of Heat Transfer*, 105(3), 1983, 465-468.
- [63] Moulic, S.G., Yao, L.S., Mixed convection along a wavy surface, *Journal of Heat Transfer*, 111, 1989, 974-979.
- [64] Elgazery, N.S., An implicit-Chebyshev pseudospectral method for the effect of radiation on power-law fluid past a vertical plate immersed in a porous medium, *Communications in Nonlinear Science and Numerical Simulation*, 13(4), 2008, 728-744.
- [65] Jang, J.H., Yan, W.M., Transient analysis of heat and mass transfer by natural convection over a vertical wavy surface, *International Journal of Heat and Mass Transfer*, 47(17-18), 2004, 3695-3705.
- [66] He, J.H., Elgazery, N.S., Abd Elazem, N.Y., Magneto-radiative gas near an unsmooth boundary with variable temperature, *International Journal of Numerical Methods for Heat and Fluid Flow*, 32(11), 2022, 545-569.
- [67] Elbarbary, E.M.E., El-Sayed, S.M., Higher order pseudospectral differentiation matrices, *Applied Numerical Mathematics*, 55(4), 2005, 425-438.

ORCID iD

Ji-Huan He  <https://orcid.org/0000-0002-1636-0559>

Nasser S. Elgazery  <https://orcid.org/0000-0003-4691-2526>

Nader Y. Abd Elazem  <https://orcid.org/0000-0003-4625-0358>



© 2023 Shahid Chamran University of Ahvaz, Ahvaz, Iran. This article is an open access article distributed under the terms and conditions of the Creative Commons Attribution-NonCommercial 4.0 International (CC BY-NC 4.0 license) (<http://creativecommons.org/licenses/by-nc/4.0/>).

How to cite this article: He J.H., Elgazery N.S., Abd Elazem N.Y. Gold Nanoparticles' Morphology Affects Blood Flow near a Wavy Biological Tissue Wall: An Application for Cancer Therapy, *J. Appl. Comput. Mech.*, 10(2), 2024, 342-356. <https://doi.org/10.22055/jacm.2023.44567.4242>

Publisher's Note Shahid Chamran University of Ahvaz remains neutral with regard to jurisdictional claims in published maps and institutional affiliations.

